The membrane-integrated steric chaperone Lif facilitates active site opening of *Pseudomonas aeruginosa* lipase A

Neha Verma[1], Peter Dollinger[2], Filip Kovacic[2], Karl-Erich Jaeger[2,3], and Holger Gohlke[1,4 *]

[1]Institute for Pharmaceutical and Medicinal Chemistry, Heinrich Heine University Düsseldorf, 40225 Düsseldorf, Germany

[2]Institute of Molecular Enzyme Technology, Heinrich Heine University Düsseldorf, Forschungszentrum Jülich GmbH, 52426 Jülich, Germany

[3]Institute of Bio- and Geosciences IBG-1: Biotechnology, Forschungszentrum Jülich GmbH, 52426 Jülich, Germany

[4]John von Neumann Institute for Computing (NIC), Jülich Supercomputing Centre (JSC) and Institute for Complex Systems - Structural Biochemistry (ICS-6), Forschungszentrum Jülich GmbH, 52426 Jülich, Germany

Running title: Lif facilitates active site opening in LipA

Keywords: protein folding, activation, potential of mean force, molecular dynamics simulations, rigidity analysis

[*]Address: Universitätstr. 1, 40225 Düsseldorf, Germany.

Phone: (+49) 211 81 13662, Fax: (+49) 211 81 13847

E-mail: gohlke@uni-duesseldorf.de

Abstract

Lipases are essential and widely used biocatalysts. Hence, the production of lipases requires a detailed understanding of the molecular mechanism of its folding and secretion. Lipase A from *Pseudomonas aeruginosa, Pa*LipA, constitutes a prominent example that has additional relevance because of its role as a virulence factor in many diseases. *Pa*LipA requires the assistance of a membrane-integrated steric chaperone, the lipase-specific foldase Lif, to achieve its enzymatically active state. However, the molecular mechanism of how Lif activates its cognate lipase has remained elusive. Here, we show by molecular dynamics simulations at the atomistic level and potential of mean force computations that Lif catalyzes the activation process of *Pa*LipA by structurally stabilizing an intermediate *Pa*LipA conformation, particularly a β-sheet in the region of residues 17-30, such that the opening of *Pa*LipA's lid domain is facilitated. This opening allows substrate access to *Pa*LipA's catalytic site. A surprising and so far not fully understood aspect of our study is that the open state of *Pa*LipA is unstable compared to the closed one according to our computational and *in vitro* biochemical results. We thus speculate that further interactions of *Pa*LipA with the Xcp secretion machinery and/or components of the extracellular matrix contribute to the remaining activity of secreted *Pa*LipA.

Introduction

P. aeruginosa lipase A (*Pa*LipA) requires the assistance of a membrane-integrated steric chaperone, the lipase-specific foldase Lif, to achieve its enzymatically active state. Here, we show by unbiased and biased molecular dynamics simulations at the atomistic level and potential of mean force computations that Lif catalyzes the activation process of *Pa*LipA by structurally stabilizing an intermediate *Pa*LipA conformation. *Pa*LipA is an important and widely used enzyme in synthetic applications because it catalyzes the hydrolysis and synthesis of a broad range of substrates.[1,2] Like other lipases, *Pa*LipA has a core structure comprised of the α/β-hydrolase fold, an active site with the catalytic triad consisting of Ser82, His251, and Asp229, and an oxyanion hole formed by Met16 and His83.[1] A characteristic feature of many lipases is "interfacial activation", which describes the fact that lipase activity increases in the presence of insoluble substrates that form an emulsion.[3] In the closed or inactive state, the active site of these lipases is covered by a lid, and this lid opens upon binding of the lipases to a hydrophobic interface.[4] *Pa*LipA possesses a lid formed by α-helix 5 but does not show "interfacial activation".[5] Rather, the production of enzymatically active *Pa*LipA is a complex process involving about 30 proteins for proper folding and extracellular secretion.[6] In a critical step, *Pa*LipA requires the assistance of an inner membrane-bound steric chaperone, the lipase-specific foldase Lif, for its conversion into an open conformation, which is also active.[7] Subsequently, *Pa*LipA is secreted to the extracellular medium *via* the type II secretion pathway using the Xcp machinery.[8] Without Lif, *Pa*LipA only folds to a near-native, but non-active state.[9,10]

Lif belongs to a small class of steric chaperones that act by lowering the energy barrier between a near-native state and an active state of the target protein.[9] Lif proteins catalyze the folding process by imprinting the essential steric (structural) information onto the target protein.[11] In that respect, steric chaperones differ from classical molecular chaperones, which indirectly increase the folding efficiency by preventing off-pathway interactions for newly synthesized proteins.[11] Most remarkably, the active state of enzymes that need specific steric chaperones is less or only marginally more stable than the inactive intermediate state.[12] However, the molecular mechanism of how these Lif proteins activate their cognate lipases has remained elusive.

A crystal structure of the complex of the homologous *Burkholderia glumae* lipase with its specific foldase (Lif:*Bg*LipA) (PDB code: 2ES4)[13] revealed that the core structure of the lipase

is virtually identical to that of the **c**losed conformation of *B. glumae* LipA (*Bg*LipA$_c$) (PDB code: 1QGE)[14] and the **o**pen state of *Pa*LipA (*Pa*LipA$_o$) (PDB code: 1EX9)[1]. The circular dichroism spectrum of the *Bg*LipA$_c$ was found indistinguishable to that of the active *Bg*LipA, which indicates no major change in secondary structure upon activation.[9] Yet, major differences were found in two key regions: first, the lid domain (helix 5) and neighboring loops (residues 109-163) occlude the active site in *Bg*LipA$_c$ and the Lif:*Bg*LipA complex but are more distant from the active site in the *Pa*LipA$_o$ structure (Figure 1A). Furthermore, helix 5 is longer by ten residues at the N-terminal end (residue 125-148) in *Pa*LipA$_o$ than in *Bg*LipA$_c$ (residues 135 -148). Second, residues 17-30 form a partial β-sheet structure in the Lif:*Bg*LipA complex and *Pa*LipA$_o$, while they form a loop in *Bg*LipA$_c$. Residues 17-30 contribute to the formation of the active site surface in *Pa*LipA$_o$, and the partial β-sheet formation (residues 21-26) likely stabilizes neighboring loops (residues 17-20 and 27-32) (Figures 1B and 1C). Together, these observations led us to hypothesize that the foldase-bound *Bg*LipA is in an intermediate conformation where partial β-sheet formation has occurred but not yet lid opening, this conformation can be considered a "loaded spring" ready to change to the open conformation.

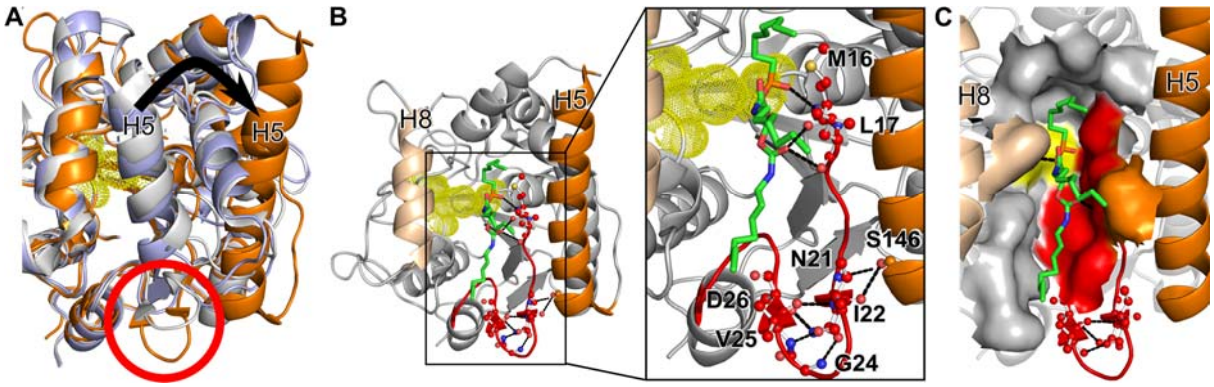

Figure 1. Structural superimposition of *B. glumae* lipase A (*Bg*LipA) and *P. aeruginosa* lipase A (*Pa*LipA) and schematic view of the active site. (A) Overlay of *Bg*LipA extracted from the foldase:lipase complex of *B. glumae* (gray, PDB code: 2ES4), closed *Bg*LipA (*Bg*LipA$_c$) (blue, PDB code: 1QGE), and *Pa*LipA in the open conformation (*Pa*LipA$_o$) (orange, PDB code: 1EX9). Extracted *Bg*LipA shows a partial β-sheet structure of region 17-30 residues, which is also present in the *Pa*LipA$_o$ structure but absent in the *Bg*LipA$_c$ structure (red circle). In contrast, helix 5 (H5) resembles the closed state by occluding the active site (yellow) in both conformations of *Bg*LipA but is moved away in *Pa*LipA$_o$, indicated by the black arrow. **(B)** *Pa*LipA$_o$ bound to an octyl-phosphinic acid 1,2-bis-octylcarbamoyloxy-ethyl ester (OCP) inhibitor (green sticks) is shown to visualize the active site (PDB code: 1EX9). H5 is shown in orange, helix 8 (H8) in wheat, and residues 17-30 in red. The catalytic triad is shown as yellow dots. The close-up view of the binding site (right inlay) shows that residues 17-30 form multiple intramolecular polar interactions in the region of partial β-sheet formation (residues 21-26). M16 forms

the oxyanion hole. **(C)** As in panel B but with a surface representation of the binding site to show that H5, H8, and residues 17-30 contribute to the formation of the active site surface.[1]

We probed this hypothesis by unbiased and biased molecular dynamics (MD) simulations followed by configurational free energy computations, complemented by *in vitro* biochemical experiments for validation. Our results indicate that Lif catalyzes the activation process of *Pa*LipA by structurally stabilizing the intermediate conformation, which facilitates the opening of the lid domain.

Methods

Generation of starting structures

The three-dimensional structure of *Pa*LipA in the closed conformation (*Pa*LipA$_c$) and complex with its foldase Lif (Lif:*Pa*LipA) is currently unknown. Thus, the homology model of *Pa*LipA$_c$ as well as the Lif:*Pa*LipA complex were constructed using the crystal structure of *B. glumae* lipase in complex with its foldase (PDB code: 2ES4) (sequence identity/similarity: 41%/73% for *Pa*LipA and 39%/52% for Lif) and the open *Pa*LipA (*Pa*LipA$_o$) (PDB code: 1EX9) as the templates. The Phyre2 web server[15] was used for homology modeling, followed by ten rounds of energy minimization with the GROMOS96 43B1 force field implemented in Swiss-PdbViewer.[16] The best model obtained was re-evaluated by using our in-house model quality assessment program TopScore.[17] The starting structure of *Pa*LipA$_o$ was obtained from the coordinates of the X-ray structure (PDB code: 1EX9).

Molecular dynamics simulations

All-atom MD simulations were performed with the Amber14 software package[18], using the ff14SB force field[19] as done previously by us.[20] *Pa*LipA$_c$, the Lif:*Pa*LipA complex, and *Pa*LipA$_o$ were placed in truncated octahedral periodic boxes of TIP3P water molecules, respectively.[21] The Particle Mesh Ewald (PME) method[22] was used to treat long-range electrostatic interactions and the SHAKE algorithm[23] to constrain the length of bonds to hydrogen atoms. A time step of 2 fs was used with a non-bonded cut-off of 8 Å. Initially, the starting structures were energy minimized by applying 50 steps of steepest descent, followed by 450 steps of conjugate gradient minimization. During the initial minimization, harmonic restraints with a force constant of 25 kcal mol^{-1} Å^{-2} were applied to the solute atoms and then reduced to 5 kcal mol^{-1} Å^{-2}. The systems were heated from 100 K to 300 K for thermalization by MD simulations in the canonical (NVT) ensemble, using the weak-coupling algorithm for

temperature control[24], carried out for 50 ps and using a force constant of 5 kcal mol^{-1} Å^{-2}. Afterward, MD simulations of 250 ps length were performed using isothermal-isobaric (NPT) ensemble MD simulations using the isotropic Berendsen barostat[24] with the same force constant in order to adjust the density of the system. Then, the force constant of the harmonic restraints was reduced to zero, and MD simulations in the NVT ensemble were carried out for 100 ps. Finally, six production MD simulations of 1 µs length each were performed for each of the three systems in the NVT ensemble using the weak-coupling algorithm for temperature control[24] with a coupling parameter $\tau = 1$ ps. To ensure the independence of the simulations, production runs were performed at temperatures of 300.0 K + T, where T was varied by 0.1 K from 0.0 to 0.5 K, respectively.[25]

Potential of mean force computations

For the potential of mean force (PMF) computations, the transition pathway of H5 between the open and closed conformations was taken from the unbiased MD simulations of *Pa*LipA$_o$. The start and end conformations of *Pa*LipA with closed and open lid were selected based on the distance between the centers of mass (D_{COM}) of the lid domain (H5, residues 125-148) and H8 (residues 210-222), which is 11.6 Å (minimum distance found during MD simulations) in the closed state and 20.6 Å in the open state. The closed state resembles the homology model of *Pa*LipA$_c$ (D_{COM} = 13.3 Å), and the crystal structure of *Pa*LipA$_o$ was taken as the open state.
The free energy profile of the opening of the active site was calculated for the *Pa*LipA structure and the Lif:*Pa*LipA complex, using umbrella sampling MD simulations in combination with the WHAM method.[26] D_{COM} was used as a reaction coordinate. Umbrella sampling MD simulations were performed along the reaction coordinate between 11.6 Å and 20.6 Å in intervals of 1 Å, applying a harmonic potential with a force constant of 2 kcal mol^{-1} Å^{-2} to tether the conformations to the respective reference point. This resulted in 10 umbrella sampling simulations per system, each 650 ns long. The first 50 ns were excluded from the subsequent WHAM analysis. The errors of the PMF profiles at the reference points were computed by applying the Monte Carlo bootstrapping analysis as implemented in WHAM using 400 resampling trials.

Analysis of trajectories

The unbiased MD trajectories were analyzed with the Amber module CPPTRAJ.[27] For each system, the average β-sheet propensity and D_{COM} were calculated; the former was calculated for residues 17-30 using the DSSP command. Additionally, the unbiased MD-generated conformations of *Pa*LipA$_c$, Lif:*Pa*LipA, and *Pa*LipA$_o$ were clustered with respect to D_{COM}. For the cluster analysis, the hierarchical agglomerative algorithm was used. A maximal distance between all members of two clusters (complete linkage) of 4 Å was used as ending criterion for the clustering. With these settings, we obtained a total of five clusters for each system. For the alignment of the structures onto the respective starting structures, root mean square fitting was done on the core residues (1-108 and 164-285) of *Pa*LipA for all systems.

Likewise, configurations *t* obtained by umbrella sampling in the windows corresponding to states I-III (see below for a definition of these states) were analyzed. To "unbias" these configurations, a weight w_t according to eqs 7 and 8 from ref.[28] was computed as done previously by us.[29] The reweighting is performed over the entire ensemble of each system and, then, w_t is normalized with respect to the sum of all w_t of each system. Finally, to identify interactions between residues in Lif and the key regions of *Pa*LipA, the average Cα-Cα distance matrix was calculated for Lif:*Pa*LipA over the six unbiased trajectories. An interaction is considered formed between respective two residues if the distance is < 10 Å, considering that the average length of the side chain is 3.5 Å for an amino acid.

Statistical analysis

Results for the β-sheet propensity of each residue and the Cα-Cα distance matrix computed from six unbiased MD simulations are expressed as arithmetic mean ± standard error of the mean (SEM). The overall SEM was calculated using the law of error propagation (eq. 1)

$$\mathrm{SEM}_{total} = \sqrt{\mathrm{SEM}_1^2 + \mathrm{SEM}_2^2 + \cdots + \mathrm{SEM}_6^2} \qquad \text{(eq. 1)},$$

where SEM_i is the SEM over each trajectory *i*. Following ref.[30], SEM_i was computed considering the decorrelation time of the examined variable. To analyze if averaged β-sheet propensities are statistically significantly different between systems, the Student's *t*-test[31] was applied, *p*-values < 0.05 and 0.001 are indicated as "*" and "**" in figures, respectively. The statistical analysis was performed using the R software.[32]

Cloning, protein production, and purification

The expression plasmid encoding *Pa*LipA and Lif was created by PCR using the Phusion High-Fidelity DNA polymerase (Thermo Fischer Scientific) in whole plasmid amplification designed for the SLIC method.[33] pLipA-SS and pEHTHis19 plasmids were used as templates for *Pa*LipA and Lif, respectively. For Lif, amino acids 1-65 were deleted using primers Lif_dLinkVD_fw and Lif_dLinkVD_rv. The expression plasmid for the *Pa*LipA variant with mutation S82A was created by whole plasmid PCR amplification with mutagenic oligonucleotide pair LipA_S82A_FW/LipA_S82A_RV designed for the SLIC method. *Pa*LipA, *Pa*LipA$_{S82A}$, and Lif were expressed in *E. coli* BL21 (DE3) using the T7-expression system with the respective plasmids. Lif was purified by immobilized metal affinity chromatography according to the modified protocol of Hausmann *et al*.[34] Cells expressing insoluble inclusion bodies of *Pa*LipA or *Pa*LipA$_{S82A}$ were suspended in Tris-HCl buffer (100 mM, pH 7) containing 5 mM EDTA and 1 mM Tris(2-carboxyethyl)phosphine (TCEP) and disrupted with a French press. Inclusion bodies were collected by centrifugation at 10,000 *g* for 10 min and suspended in the same buffer. Centrifugation and wash steps were repeated three times to obtain purified inclusion bodies. The purified inclusion bodies were suspended in a small amount of water and, afterward, 8 M urea (0.5 ml / 100 ml culture volume) was added. The inclusion bodies were incubated for 1 h at 37°C or until all inclusion bodies have been dissolved.

In vitro activation of *Pa*LipA with Lif.

Chemically denatured *Pa*LipA and *Pa*LipA$_{S82A}$ inclusion bodies were renatured by fast, at least 100-fold, dilution of the denaturant with ice cold 10 mM TG (5 mM TRIS, 5 mM glycine, pH 9) containing an equimolar amount of Lif followed by overnight incubation at 4°C.

Lipase activity assay

Para-nitrophenyl palmitate (*p*NPP, 1 mM) was used as a substrate in 10 mM TG buffer containing 1 mM $CaCl_2$ to determine lipolytic activities.[35] The release of *p*-nitrophenolate was monitored spectrophotometrically.

Protein stability determination by differential scanning fluorimetry

Lif:*Pa*LipA and Lif:*Pa*LipA$_{S82A}$ complexes prepared as described above were loaded into the measuring capillaries (Prometheus NT.Plex nanoDSF Grade Standard Capillary Chips) from a

384-well microtiterplate and were heated from 15°C to 95°C (heating rate of 0.2°C/min). The emission shift over temperature (F) was recorded at 330 nm and 350 nm using the Prometheus NT.Plex nanoDSF device (Nano Temper, Munich, Germany). The PR.ThermControl software provided by the company was used to calculate the ratio of $F_{350\ nm}$ and $F_{330\ nm}$ and its first derivative.

Constraint network analysis

To quantify a change in structural rigidity of *Pa*LipA upon binding to Lif, we employed a perturbation approach[36] using the Constrained Network Analysis (CNA) methodology[37], as described previously.[38] Briefly, CNA is a graph theory-based tool for rigidity analysis and has successfully been applied to a number of problems.[39-41] In a perturbation approach, the rigidity analysis is compared before (ground state) and after perturbing the constraint network by removing constraints of the residues of interest. For the perturbation analysis, first, an ensemble of network topologies was generated from MD snapshots of the Lif:*Pa*LipA complex, sampled at 2 ns intervals from the six unbiased MD simulations of 1 µs length each. Second, Lif residues forming interactions with the key regions in *Pa*LipA were identified from the average Cα-Cα distance matrix as described above. Third, for each of the identified residues *i* in Lif (residues 195-203, 213,217-220), the perturbation was performed, which resulted in a per-residue perturbation free energy $\Delta G_{i,\mathrm{CNA}}$ following a linear response approximation (eq. 2):

$$\Delta G_{i,\mathrm{CNA}} = \alpha(\langle E_{i,\mathrm{CNA}}^{perturbed}\rangle - \langle E_{i,\mathrm{CNA}}^{ground}\rangle) \quad (2)$$

α was set to 0.02 as in ref.[36]

Results

Structural dynamics of the lid of free *Pa*LipA and when bound to Lif

Initially, we aimed at analyzing the tendency of closed *Pa*LipA (*Pa*LipA$_c$) free and in complex with Lif (Lif:*Pa*LipA) to move towards the open state, and of free open *Pa*LipA (*Pa*LipA$_o$) towards the closed state, by unbiased MD simulations. Due to the absence of respective crystal structures, *Pa*LipA$_c$ and Lif:*Pa*LipA were built by homology modeling (Figures 2A-C). The models were assessed with our in-house model quality assessment program TopScore[17] and found to be 68 % correct for *Pa*LipA and 52 % correct for Lif. The correctness of the model is computed as the predicted global and local lDDT score[42], which compares all intra-molecular heavy-atom distances within two structures. If all distances deviate by more than 4 Å, the two structures are considered entirely different, and they are considered completely identical if all distances deviate by less than 0.5 Å. As the native structure is not known, the score is predicted by a deep neural network, which was trained on a large dataset of 660 protein targets totaling over 1.33×10^5 models and over 1.9×10^7 residues. It uses model quality predictions from different sources as input, including an agreement between features predicted from the sequence and measured in the model, such as secondary structure, solvent accessibility, and residue contacts.

First, we analyzed the MD simulations with respect to the average β-sheet propensity of residues 17-30 of *Pa*LipA because this secondary structure type is a characteristic feature of *Pa*LipA$_o$. For the Lif:*Pa*LipA complex, the likelihood of β-sheet formation is highest (96.5 ± 0.8%, mean ± SEM) (Figure 2D). In contrast, *Pa*LipA$_c$ showed a significantly lower β-sheet propensity of 41.1 ± 12%. This result indicates that Lif fosters the formation of the β-sheet structure. As expected, *Pa*LipA$_o$ exhibits a β-sheet propensity more similar to that of the Lif:*Pa*LipA complex (83.5 ± 3.5%), yet, the significantly smaller value suggests that *Pa*LipA$_o$ tends to move towards the closed conformation.

Next, we computed D_{COM} between H5 and H8 over the MD simulations to measure the opening and closing of the active site. Starting from *Pa*LipA$_c$, pronounced fluctuations of D_{COM} were observed that encompass both partially open lid conformations ($D_{COM} \approx 16$ Å) and more closed ones ($D_{COM} \approx 10$ Å) compared to the starting state ($D_{COM} = 13.3$ Å) (Figure 2E). A similar behavior was observed for *B. cepacia* lipase during MD simulations in water.[43] Starting with the Lif:*Pa*LipA complex, the probability density of partially open conformations ($D_{COM} \approx 16$ Å) was ~2-fold higher than for *Pa*LipA$_c$ (Figure 2E). This suggests that *Pa*LipA

in complex with Lif has a stronger tendency to move towards the partially open state than *Pa*LipA$_c$, although this tendency is obvious in only three trajectories out of six. As when starting from the closed conformation of *Pa*LipA, further closing of the lid was also observed during the MD simulations of the complex. Finally, starting from *Pa*LipA$_o$, the partially open state becomes most populated ($D_{COM} \approx 16$ Å), and even closed conformations ($D_{COM} \leq 13.3$ Å) were found (Figure 2E). Likewise, for *B. cepacia* lipase, an open-to-closed transition of the lid during MD simulations in water was found.[44]

To get an atomistic view on the further closed and partially open states observed in the above probability density distributions, we clustered the structures generated from the six MD trajectories for each system with respect to D_{COM}, using a threshold value of 4 Å. The two most populated clusters obtained respectively (Figure S1) were analyzed as to conformational changes in the lid domain. For *Pa*LipA$_c$ and the Lif:*Pa*LipA complex, the most populated clusters were dominated by structures with further closed active site ($D_{COM} < 13.3$ Å) (Figure S1A and S1C). In the second most populated clusters, in addition to lid movement towards larger D_{COM} values showing a partial opening of the active site, we also observed the formation of an additional α-helical structure for H5 of *Pa*LipA$_c$ and *Pa*LipA in complex with Lif (Figure S1B and S1D). For *Pa*LipA$_o$, the representative structures of the two most populated clusters ($D_{COM} \approx 16.2$ Å for the first and $D_{COM} \approx 13.9$ Å for the second, respectively (Figure S1E and S1F)) show a decrease and a bent in α-helix structure of H5 similar to Lif:*Pa*LipA (Figure S1D) when compared to the X-ray structure of *Pa*LipA$_o$.

To conclude, the lid of *Pa*LipA shows pronounced structural fluctuations on the μs time scale, reaching also a partially open state when starting from either a closed or open state. When starting from the closed state, reaching the partially open state is more favored for *Pa*LipA when bound to Lif.

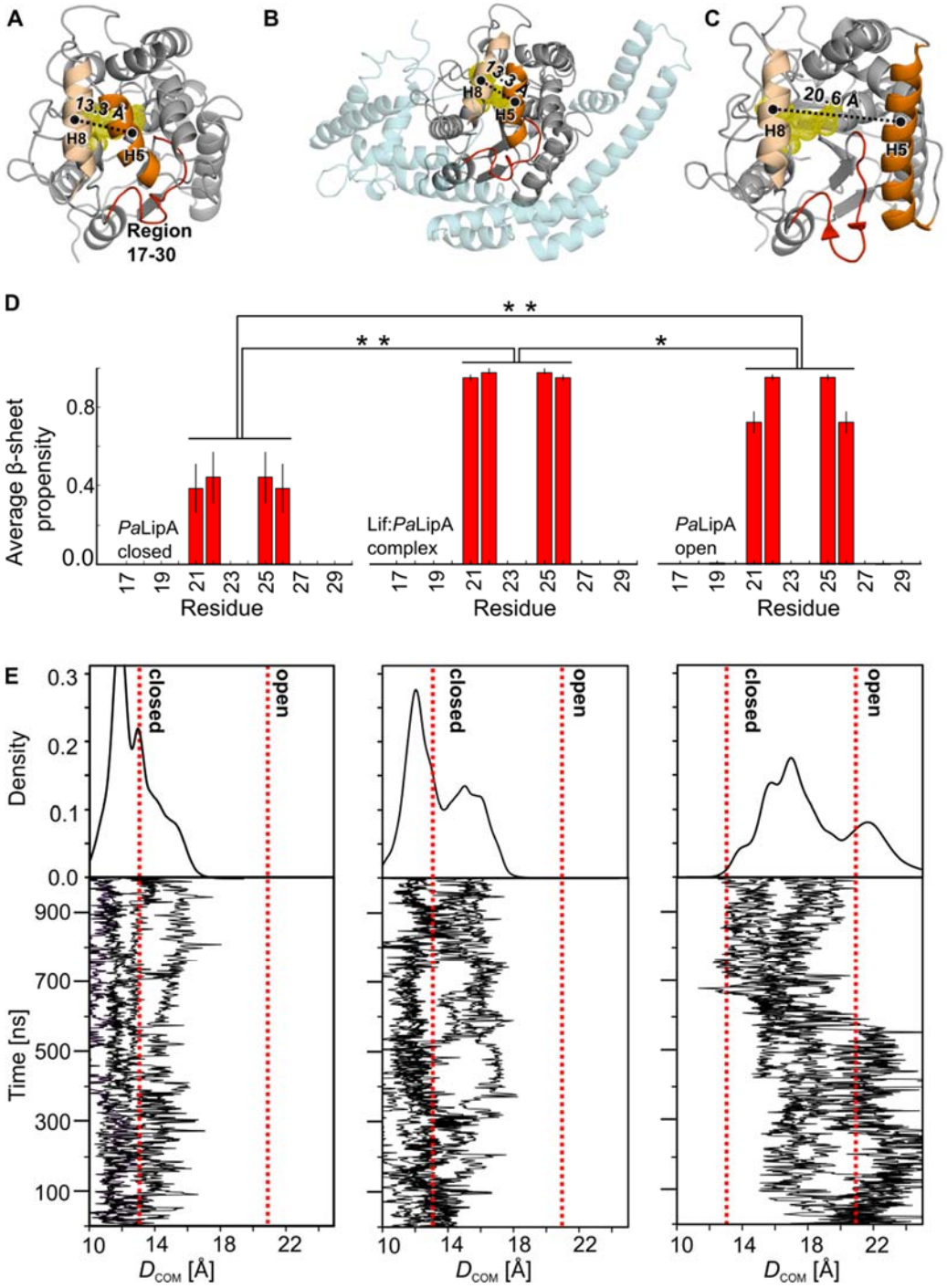

Figure 2. Structural dynamics of *Pa*LipA during unbiased MD simulations. (A) Structural model of *Pa*LipA in the closed conformation (*Pa*LipA$_c$) generated by homology modelling. Active site residues (catalytic triad residues S82, H251, and D229) are shown as yellow dots, which are covered by the lid domain (H5) (orange). H8 is highlighted in wheat. D_{COM} is represented by a black, dotted line. In *Pa*LipA$_c$, D_{COM} = 13.3 Å. Residues 17-30 are shown in red and do not exhibit the partial β-sheet structure, which is a characteristic feature of *Pa*LipA$_o$. **(B)** Homology model of the closed *Pa*LipA in complex with Lif (Lif:*Pa*LipA), Lif is represented in cyan, otherwise the representation is as in (A). **(C)** Crystal structure of *Pa*LipA$_o$ (PDB code: 1EX9), represented as in (A). H5 moved away from the active site, and D_{COM} = 20.6 Å (black dotted line). The residues 17-30 form a partial β-sheet structure (red). **(D)** Average per-residue β-sheet propensities of residues 17-30 starting from *Pa*LipA$_c$ (left),

Lif:*Pa*LipA (middle), and *Pa*LipA$_o$ (right). Error bars indicate SEM (eq. 1) and statistically significant differences of the averages calculated with the Student's *t*-test were indicated by "*" *p*-values < 0.05 and "**" *p*-values < 0.001. **(E)** D_{COM} over the simulation times of six MD trajectories each for the three systems listed in (D). Additionally, the probability densities are shown. Red dotted lines indicate the D_{COM} values of the open and closed *Pa*LipA states.

The open state of *Pa*LipA is more favorable when bound to Lif

To complement the unbiased MD simulations, we computed the potential of mean force (PMF) of the opening of the active site in free *Pa*LipA and complex with Lif (Lif:*Pa*LipA), applying umbrella sampling and using D_{COM} (Figure 2A) as a reaction coordinate. The PMF computations were performed for a plausible transition path of H5 obtained from unbiased MD simulations of *Pa*LipA$_o$ (see Methods section for details). Approximately Gaussian-shaped frequency distributions were obtained for each reference point along the reaction coordinate, with well overlapping windows (Figure S2). Such distributions are a prerequisite for the successful application of WHAM to compute a PMF.[26] Repeating the PMF computations for parts of the simulation time demonstrates that, for both systems, the PMFs are converged after at most 550 ns of simulation time per window (maximal difference between any two PMFs after a simulation time of 550 ns: 0.1 kcal mol^{-1}) (Figure S3). Usually, high configurational entropy results in the delayed convergence of the PMF.[45] Along these lines, our unbiased MD simulations reveal that the lid of *Pa*LipA fluctuates markedly on the µs time scale (Figure 2E). Furthermore, during lid opening, helix formation in the region of residues 125 – 135 takes place, as also indicated from the comparison of the open and closed structures (Figure 1A and 1C). Helix formation occurs on the time scale of hundreds of ns.[46,47] Both effects likely contribute that at most 550 ns per window are required to achieve converged PMFs. For comparison, the PMF values at the smallest D_{COM} sampled (11.6 Å) were set to zero in both cases (Figure 3A).

Although in both cases the configurational free energy increases with increasing D_{COM}, the PMFs differ in their global shape: The PMF of the Lif:*Pa*LipA complex increases more moderately than that of *Pa*LipA and shows broader local minima (Figure 3A). In more detail, the global energy minima (state I) for both free *Pa*LipA and the Lif:*Pa*LipA complex are found for the closed state (D_{COM} = 12.4 Å and 13.2 Å, respectively, $\Delta G \approx 0$ kcal mol^{-1} with respect to D_{COM} = 11.6 Å). At $D_{COM} \approx$ 14.8 Å, both PMFs have a local minimum (state II) of similar height ($\Delta G \approx 1$ kcal mol^{-1}). The corresponding energy well of the Lif:*Pa*LipA complex is extended until $D_{COM} \approx$ 16 Å. In contrast, the PMF for *Pa*LipA rises steeply immediately

following the local minimum. This finding coincides with a higher population of partially open structures found for Lif:*Pa*LipA in the unbiased simulations. Finally, flat PMF regions are found for both systems at $D_{COM} \approx 20.6$ Å (state III), but the configurational free energies with respect to the global minimum differ (Lif:*Pa*LipA: $\Delta G \approx 2.9$ kcal mol^{-1}, *Pa*LipA: $\Delta G \approx 4.6$ kcal mol^{-1}).

Furthermore, we computed the average β-sheet propensity of residues 17-30 of *Pa*LipA with and without Lif over the reweighted (unbiased) (Figure S4; see Methods section and ref. [28]) configurations from umbrella sampling for states I-III, respectively (Figure 3B). At the global minimum (state I), the β-sheet propensity averaged over windows 1 and 2 is significantly lower for *Pa*LipA (~21 ± 6%) than in state II, averaged over windows 3 and 4, and state III, averaged over windows 9 and 10 (~ 60 ± 4% and ~ 63 ± 3%, respectively). In contrast to *Pa*LipA, in Lif:*Pa*LipA, state I (~ 94 ± 0.8%) has a similar β-sheet propensity as state II and state III (~ 75 ± 2% and 84 ± 1%, respectively). The difference between the average β-sheet propensities of states I of *Pa*LipA and Lif:*Pa*LipA is highly statistically significant ($p < 0.001$). Similarly, for states II and III, the respective average β-sheet propensities of Lif:*Pa*LipA are significantly higher than those of *Pa*LipA ($p < 0.05$ for both states).

To conclude, the PMF computations reveal that the open state of *Pa*LipA is disfavored compared to the closed state but that in Lif:*Pa*LipA the open state is 1.7 kcal mol^{-1} more favorable than in *Pa*LipA. Furthermore, according to unbiased configurations from the umbrella sampling simulations, binding to Lif significantly favors the formation of the β-sheet in the region of residues 17-30, and this effect is most pronounced in the state I (~73 fold increase in the propensity).

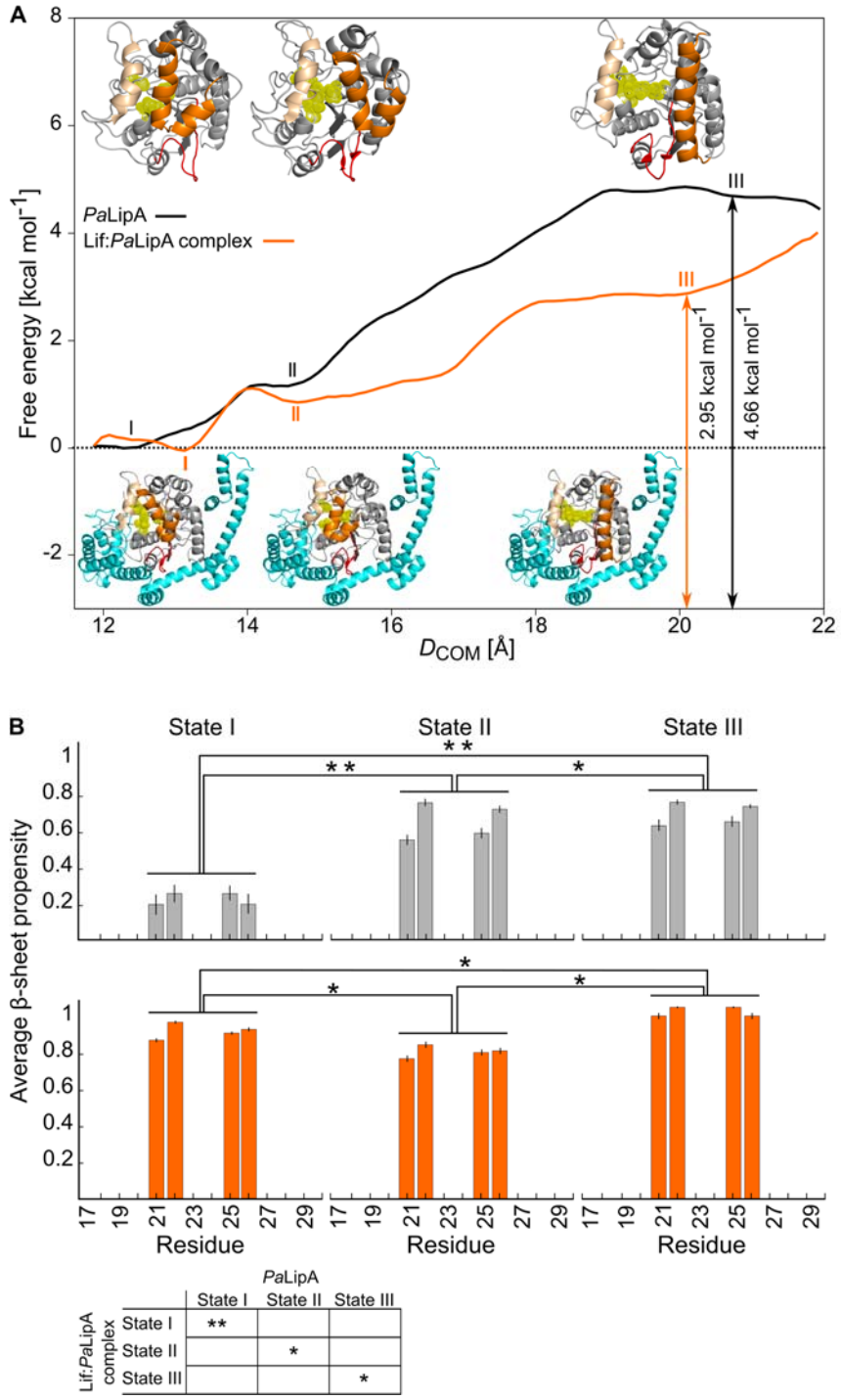

Figure 3. PMF computation of the active site opening in *Pa*LipA and the Lif:*Pa*LipA **complex and average β-sheet propensities of residues 17-30 of *Pa*LipA with and without Lif for three states identified in the PMFs. (A)** Configurational free energies of active site opening of *Pa*LipA as a function of D_{COM} used as a reaction coordinate for free *Pa*LipA (black) and the Lif:*Pa*LipA complex (orange). The standard deviation for all data points is < 0.002 kcal mol^{-1} computed by bootstrap analysis. Roman numbers indicate the identified states. Representative structures for states I-III are shown as cartoons for *Pa*LipA (top) and Lif:*Pa*LipA complex (bottom), respectively. The PMF values at D_{COM} = 11.6 Å were set to zero, respectively. **(B)** Per-residue averaged β-sheet propensity for residues 17-30 of *Pa*LipA, calculated across the umbrella sampling windows corresponding to the states I-III as described in (A), using reweighted (unbiased) configurations for *Pa*LipA (top) and the

Lif:*Pa*LipA complex (bottom). The table at the bottom displays results from comparing β-sheet propensities between *Pa*LipA and Lif:*Pa*LipA. Error bars indicate the SEM (eq. 1) and asterisks statistically significant differences (see Methods section for definition).

*Pa*LipA released from Lif loses its lipolytic activity over time under *in vitro* conditions

The unbiased MD simulations and the PMF computations reveal that *Pa*LipA$_o$ tends to move to an at most partially open state and that the open state is energetically disfavored with respect to the closed one, respectively. Although previous computations on related systems yielded similar results[44], our results are unexpected because, in a cellular context, secreted *Pa*LipA remains active and stable as indicated by the harsh conditions required for its denaturation.[14,48,49] In order to validate our computations, we thus performed biochemical experiments to probe if *Pa*LipA activity decreases under *in vitro* conditions similar to our simulations when the lipase is released from Lif.

To do so, a catalytically inactive *Pa*LipA variant, in which amino acid S82 of the catalytic triad is mutated to alanine, was used in addition to wild type *Pa*LipA. Purified *Pa*LipA$_{S82A}$ was renatured and used for complex formation with Lif at 1 μM concentration. According to the results of thermal unfolding experiments carried out with differential scanning fluorimetry (DSF), *Pa*LipA$_{S82A}$ forms a complex with Lif that has stability similar to that of *Pa*LipA with Lif (Figure 4A). This result is concordant with the fact that S82 is buried within *Pa*LipA and does not participate in interactions with Lif. At the used concentrations, the amount of free *Pa*LipA$_{S82A}$ or *Pa*LipA and Lif should be negligible because of the high binding affinity of Lif:*Pa*LipA (K_d = 5nM).

As expected, no catalytic activity is found for the Lif:*Pa*LipA$_{S82A}$ complex, in contrast to the Lif: *Pa*LipA complex (Figure 4B). After dilution of the Lif:*Pa*LipA$_{S82A}$ complex to 1 nM, renatured *Pa*LipA was added in excess at a concentration of 100 nM, followed by 3 h incubation. The addition of *Pa*LipA to the Lif:*Pa*LipA$_{S82A}$ complex restored activity to ~90 % of that of Lif:*Pa*LipA (Figure 4B), indicating that *Pa*LipA replaces *Pa*LipA$_{S82A}$ and then becomes activated by Lif.

Finally, we performed a complementary experiment in which 50 nM Lif:*Pa*LipA complex was supplemented with 50 nM or 100 nM *Pa*LipA$_{S82A}$, and with buffer as control, followed by

determination of the catalytic activity over time (Figure 4C). After 145 min, the activity level decreased by about 15 % and 35 % in the presence of 50 nM and 100 nM *Pa*LipA$_{S82A}$, respectively, which indicates the replacement of *Pa*LipA by *Pa*LipA$_{S82A}$ and the subsequent loss of catalytic activity of free *Pa*LipA in a *Pa*LipA$_{S82A}$ concentration-dependent manner. Addition of 100 nM Lif after 150 min restored catalytic activity, demonstrating that replaced *Pa*LipA can be re-activated by Lif.

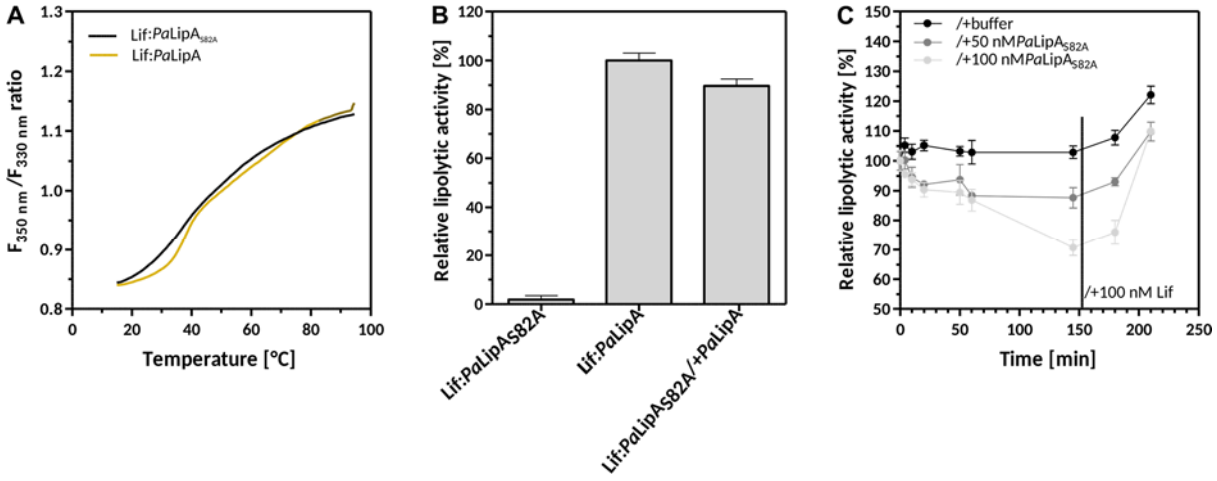

Figure 4. Dynamics of Lif:*Pa*LipA complex formation and *Pa*LipA activation. (A) DSF melting curves of the Lif:*Pa*LipA$_{S82A}$ and Lif:*Pa*LipA complexes at 1 µM concentrations. **(B)** The catalytic activity of Lif:*Pa*LipA$_{S82A}$ and Lif:*Pa*LipA (set to 100%) in comparison to Lif:*Pa*LipA$_{S82A}$ in the presence of *Pa*LipA (Lif:*Pa*LipA$_{S82A}$/+*Pa*LipA), which restores catalytic activity in the latter case. **(C)** The catalytic activity of Lif:*Pa*LipA over time in the absence (/+buffer, set to 100%) and presence of *Pa*LipA$_{S82A}$. The presence of *Pa*LipA$_{S82A}$ reduces catalytic activity in a concentration-dependent manner. The activity can be restored by addition of Lif (vertical line).

The activity decrease due to the addition of *Pa*LipA$_{S82A}$ in the first step of the experiment was lower than expected. According to the ratios of *Pa*LipA and *Pa*LipA$_{S82A}$, the expected activity decrease is 50% and 67% for the samples with 50 nM and 100 nM *Pa*LipA$_{S82A}$, respectively. The discrepancy is likely caused by incomplete complex formation at the start of the experiment and unfinished lipase exchange after 145 min. The fact that the Lif:*Pa*LipA control showed an increase in activity upon Lif addition supports the former point as does the lack of a plateau around 145 min in the case of 100 nM *Pa*LipA$_{S82A}$ and the need to incubate Lif with *Pa*LipA overnight to achieve maximal activation the latter.

To conclude, these *in vitro* experiments demonstrate that *Pa*LipA released from Lif loses its lipolytic activity over time and that the activity can be rescued by the addition of Lif. The results suggest that the closed-to-open transition of *Pa*LipA is a reversible process and that Lif

is required for the conformational transition of *Pa*LipA to the open state as well as to stabilize *Pa*LipA in the open conformation under *in vitro* conditions.

Lif binding affects the structural stability of key regions of *Pa*LipA involved in the opening of the active site

Our results suggest that Lif facilitates the opening of the active site in *Pa*LipA and stabilizes the partial β-sheet structure in the region of residues 17-30. To understand the underlying mechanism how Lif binding influences the active site opening in *Pa*LipA, we analyzed changes in the structural rigidity of *Pa*LipA upon mutating residues of Lif that interact with *Pa*LipA using an ensemble- and rigidity-theory based perturbation approach[36] integrated into the CNA approach.[37] Initially, we identified interactions between Lif and H5 as well as residues 17-30 of *Pa*LipA based on the Cα-Cα distance matrix averaged over the six unbiased MD simulations of the Lif:*Pa*LipA complex (Figure 5A). In total, 13 residues of Lif were identified (195-203, 213, 217-220) that are in direct contact with the region of residues 17-30 of *Pa*LipA (Figure 5B). By contrast, no residues of Lif were identified that interact with H5.

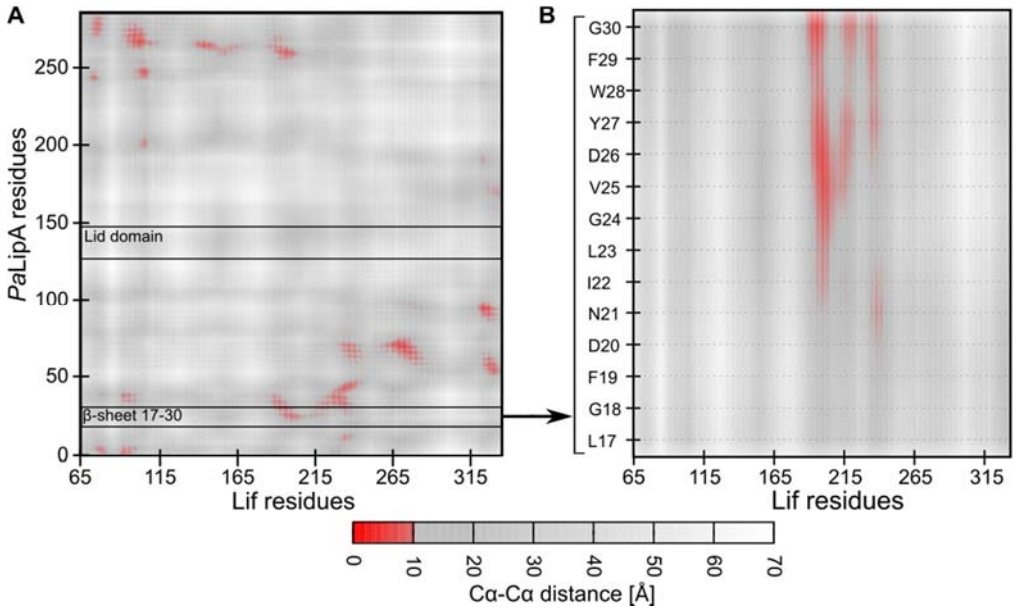

Figure 5. Lif residues interacting with *Pa*LipA. (A) Average Cα-Cα distance matrix calculated for the Lif:*Pa*LipA complex over six unbiased MD simulations of 1 µs length each. Residue pairs with a Cα-Cα distance < 10 Å are colored in red (see color scale) and considered in direct contact. Regions of H5 and residues 17-30 in *Pa*LipA are indicated by black lines. The SEM is < 0.1 Å in all cases. **(B)** Close-up of the Cα-Cα distance matrix for residues 17-30 in *Pa*LipA. Color code as in panel A.

To probe a potential influence of Lif binding on *Pa*LipA stability, first, a conformational ensemble of the Lif:*Pa*LipA complex was generated from the above shown MD simulations, constituting the ground state (see the Methods section for details). A perturbed state of the Lif:*Pa*LipA complex was then generated by removing the side chain of a Lif residue except the C_β atom, mimicking a substitution to alanine, but keeping the structures of Lif and *Pa*LipA unchanged otherwise. This perturbation was carried out separately for each of the 13 above mentioned residues. The changes are quantified as residue-wise free energy $\Delta G_{i,\mathrm{CNA}}$ (eq. 2), a measure for structural stability.[37] By definition, a change of the biomolecular conformation between the ground and perturbed states is excluded in our approach. Therefore, any observed changes in the biomolecular rigidity and flexibility must arise solely from local changes in the network topology that are due to the uncoupling of the residue side chain.[37] This procedure has been applied successfully before [37,50-52] and resembles a free energy decomposition scheme as non-perturbing alternative for (computational) alanine scanning mutagenesis.[53]

Of the 13 residues tested, F195, R199, R203, D218, and R219 showed the largest effect on the structural stability of *Pa*LipA (Figure 6, for effects on the structural stability of Lif see Figure S5, results for residues showing no effect are summarized in Figure S6). Upon perturbation of residue F195, the changes in $\Delta G_{i,\mathrm{CNA}}$ were largest for *Pa*LipA residues 15-45, which form the oxyanion hole and the cleft of the active site, whereas residue R199 affects the stability of residues 15-45 and in addition residues 255-268, which constitute the loop stabilizing the catalytic triad residue H251 (Figures 6A and 6B). Upon perturbation of residue R203, in addition to residues 15- 45, residues 142-144, which constitute the neighboring loop at the C-terminus of H5 also showed substantial changes in $\Delta G_{i,\mathrm{CNA}}$ (Figure 6C). By contrast, residues D218 and R219 specifically affected the stability of region 17-30 of *Pa*LipA (Figures 6D and 6E). Notably, all affected residues belong to the substrate binding site of *Pa*LipA which undergoes conformational rearrangements during activation. Finally, these perturbations also affect the stability of a number of the neighboring residues in Lif itself (Figure S5).

To conclude, the perturbation analysis reveals that certain Lif residues that directly interact with *Pa*LipA lead to a long-range impact on the structural stability of *Pa*LipA regions (residues 142-144, 255-268 and 15-45) in the vicinity of *Pa*LipA's active site. In particular, the stability of the partial β-sheet structure of residues 17-30 is affected, which forms upon opening of the lid domain.

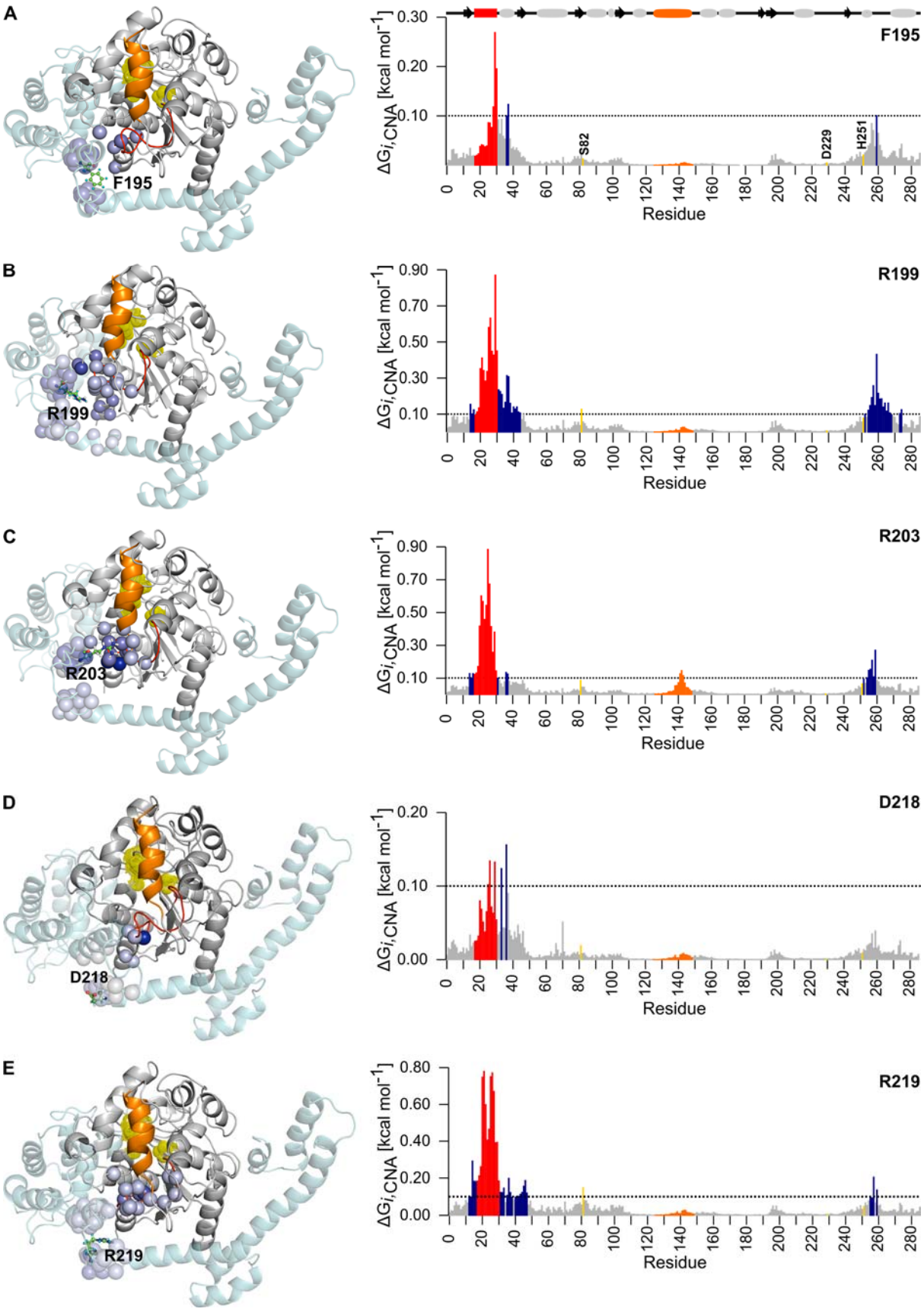

Figure 6. Potential influence of Lif residues interacting with *Pa*LipA on the structural stability of *Pa*LipA.
A perturbation approach implemented in CNA was applied on the ensemble of structures of Lif:*Pa*LipA generated

by six unbiased MD simulations. **(A)** Left: Residues with $\Delta G_{i,\mathrm{CNA}}$ above the threshold of 0.1 kcal mol^{-1} are depicted as spheres on the Lif:*Pa*LipA complex structure. Blue colors reflect predicted $\Delta G_{i,\mathrm{CNA}}$ values, the larger the value, the darker is the color. The perturbed residue F195 of Lif (green, ball-and-stick representation) influences the stability of residues 17-30 of *Pa*LipA (red). H5 (orange) is shown in closed conformation occluding the binding site (yellow). Right: The histogram shows the per-residue $\Delta G_{i,\mathrm{CNA}}$ for *Pa*LipA (see Figure S5 for $\Delta G_{i,\mathrm{CNA}}$ of Lif). The dashed line indicates the threshold value of 0.1 kcal mol^{-1} above which residues are considered affected in terms of their structural stability. Residues forming H5, the catalytic triad, and region 17-30 are highlighted in orange, yellow, and red, respectively. Other residues with $\Delta G_{i,CNA}$ above the threshold are highlighted in blue. **(B)** As in panel A for the perturbation of residue R199 of Lif. **(C)** As in panel A for the perturbation of residue R203 of Lif. **(D)** As in panel A for the perturbation of residue D218 of Lif. **(E)** As in panel A for the perturbation of R219 of Lif. The standard error of the mean is < 0.05 kcal mol^{-1} for all residues in all cases.

Discussion

In this study, we have shown by molecular simulations at the atomistic level that the steric chaperone Lif catalyzes the activation process of *Pa*LipA by structurally stabilizing an intermediate *Pa*LipA conformation, particularly a β-sheet in the region of residues 17-30, such that the opening of the lid domain is facilitated. This opening allows substrate access to *Pa*LipA's catalytic site. Our study was motivated by previous experimental work that showed that the homologous *Bg*LipA in the absence of its foldase adopts a near-native conformation, which is enzymatically inactive, however.[10] Addition of the foldase results in lipase activity in solution.[10] In the Lif:*Bg*LipA complex crystal structure, *Bg*LipA shows a partial β-sheet formation in the region of residues 17-30,[13] which has also been observed in *Pa*LipA$_o$[1] but not in closed *Bg*LipA.[14] Notably, lipase activity was also found in the crystals of the Lif:*Bg*LipA complex,[13] concordant with helix 5 of *Bg*LipA having sufficient space to move in the crystal lattice and, thus, being able to switch to the open state.[9,54]

Our result is supported by three complementary computational approaches and *in vitro* biochemical experiments. First, we performed six independent, unbiased, microsecond-long MD simulations at the atomistic level in explicit solvent starting from (free) *Pa*LipA$_c$ and *Pa*LipA$_c$ in complex with Lif (Lif:*Pa*LipA). These simulations revealed that the lid of *Pa*LipA shows pronounced structural fluctuations on the μs time scale and also reaches a partially open state when starting from either a closed or open state. Yet, when starting from the closed state, the partially open state is reached more frequently if *Pa*LipA is bound to Lif than when it is free. To our knowledge, the length of our MD simulations surpasses comparable previous ones

on *Pa*LipA by at least 800 ns,[55-57] whereas no MD simulations have been reported for Lif:*Pa*LipA complex so far. For the MD simulations, we used established parameterizations for the solvent,[21] and proteins,[19] which we had also applied successfully in other simulations on soluble proteins.[29,38,58,59] Furthermore, the impact of force field deficiencies on our results is expected to be small due to cancellation of errors when comparatively assessing simulation results for *Pa*LipA in unbound or bound state, or started from different conformations. While an experimental structure was available for *Pa*LipA$_o$,[1] homology models were used as starting structures for *Pa*LipA$_c$ and Lif:*Pa*LipA. Note that, as the partial β-sheet structure is absent in the closed *Bg*LipA structure, our homology models of *Pa*LipA$_c$ and Lif:*Pa*LipA do not have a partial β-sheet structure in the region of residues 17-30 either. Still, a much higher β-sheet propensity is found in that region in MD simulations of the Lif:*Pa*LipA complex than for *Pa*LipA$_c$, concordant with the presence of such a β-sheet in the crystal structure of Lif:*Bg*LipA and the lack of it in the crystal structure of closed *Bg*LipA. Concomitantly, MD simulations started from *Pa*LipA$_o$ exhibited a β-sheet propensity more similar to that of Lif:*Pa*LipA, although the smaller values suggested that *Pa*LipA$_o$ tends to move towards the closed conformation. Apparently, binding to Lif fosters β-sheet formation in *Pa*LipA in the region of residues 17-30.

As a second, independent approach, we investigated the energetics of active site opening in free *Pa*LipA and in the complex with Lif (Lif:*Pa*LipA) by umbrella sampling simulations followed by PMF computations, using established protocols successfully applied previously by us[58,59] and D_{COM} as an intuitive reaction coordinate previously applied on a similar system.[58] To our knowledge, the energetics of active site opening in *Pa*LipA has not been investigated by computational means before. The PMF computations reveal that the open state of *Pa*LipA is disfavored compared to the closed state but that in Lif:*Pa*LipA the open state is 1.7 kcal mol^{-1} more favorable than in *Pa*LipA. Both findings are in agreement with results from unbiased MD simulations (see above), demonstrating internal consistency of our findings. The former finding is also in agreement with our *in vitro* experiments according to which *Pa*LipA set free from Lif loses its lipolytic activity over time. Finally, evaluating the β-sheet propensity of the region of residues 17-30 on reweighted configurations from the umbrella sampling simulations confirmed that binding to Lif significantly favors β-sheet formation in that region, particularly in the closed state, again demonstrating internal consistency with respect to results from unbiased MD simulations.

Third, we applied a rigidity theory- and ensemble-based perturbation approach for analyzing biomolecular rigidity and flexibility[36,37] successfully used previously by us[38] to scrutinize the mechanism of how Lif binding influences the active site opening in *Pa*LipA. The results revealed that five out of 13 Lif residues forming contacts with the region of residues 17-30 of *Pa*LipA contribute to the structural stability of the binding site in a long-range manner, in particular the region formed by residues 17-30, the neighboring loop of the lid/H5 (residues 142-144), and the loop (residues 255-268) stabilizing H251, one of the residues of the catalytic triad. Considering that tertiary interactions can stabilize β-sheet formation,[60-62] these results can explain why a higher β-sheet propensity in the region of residues 17-30 is found when *Pa*LipA is bound to Lif.

A surprising and so far not fully understood aspect of our study is that the open state of *Pa*LipA is unstable compared to the closed one according to our computational and *in vitro* results (Figure 7). This finding does not contradict results on α-lytic protease and subtilisin, which need steric chaperones to reach their active state and whose active states are less than or only marginally more stable than the inactive intermediate states.[12,63-65] Yet, it is at variance with the fact that *Pa*LipA secreted to the extracellular medium remains active.[14,48,49] At present, we can only speculate that further interactions of *Pa*LipA with the Xcp secretion machinery and/or components of the extracellular matrix contribute to the remaining activity, e.g., by increasing the energy barrier between the open and closed states of *Pa*LipA, which is almost absent in our free energy profiles. Binding of a substrate might also stabilize the open state of *Pa*LipA. However, in this study, we address the question how the inner membrane-integrated steric chaperone Lif facilitates active site opening of *Pa*LipA. The catalytic domain of Lif is located in the periplasm, and in this compartment, the presence of substrates is unlikely. Yet, the activation of *Pa*LipA was suggested to start there already[66]. Hence, we refrained from doing additional simulations with a substrate bound, as it would not reflect the biology underlying the addressed question.

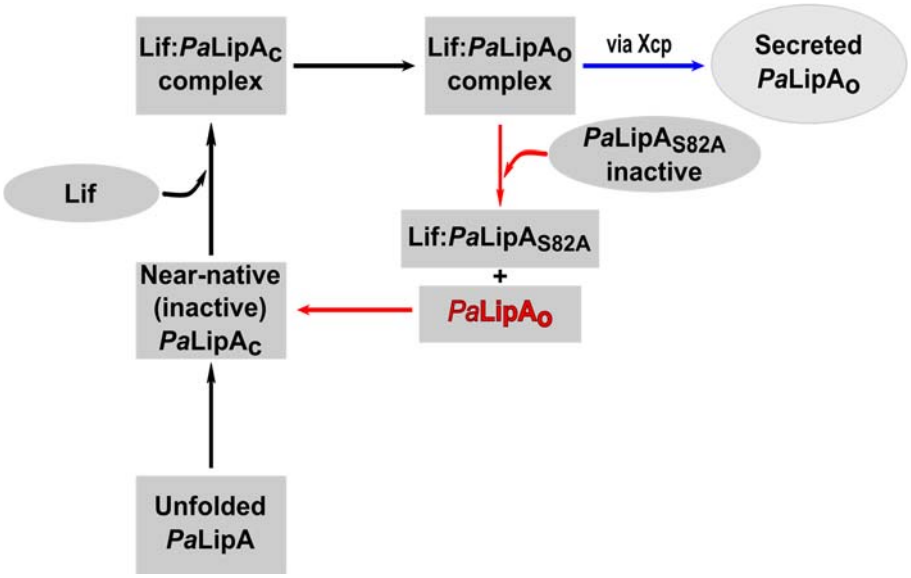

Figure 7. Proposed scheme for *Pa*LipA activation and secretion.[7,8,10] Unfolded *Pa*LipA folds to a near-native inactive state in the absence of Lif (*Pa*LipA$_c$). This *Pa*LipA$_c$ binds to Lif (Lif:*Pa*LipA$_c$) and undergoes conformational changes towards the open state (Lif: *Pa*LipA$_o$). After opening, *Pa*LipA$_o$ is released from the Lif:*Pa*LipA$_o$ complex and *in vivo* secreted to the extracellular medium via the Xcp machinery (blue arrow), although the exact mechanism of secretion is still unknown. Results from MD simulations, PMF computations, and *in vitro* experiments (red arrows) obtained in this study indicate that *Pa*LipA$_o$ released from the complex (red) by addition of the inactive variant (*Pa*LipA$_{S82A}$) can fold back to inactive *Pa*LipA$_c$. Black arrows indicate processes occurring *in vitro* and *in vivo*. Our results thus suggest that Lif is required to facilitate the closed-to-open transition of *Pa*LipA$_c$ as well as to stabilize *Pa*LipA$_o$ under *in vitro* conditions until it is secreted to extracellular medium via the Xcp machinery.

In summary, our results shed light onto the molecular mechanism of a steric chaperone in that they provide an explanation how Lif directly catalyzes the folding process of *Pa*LipA by imprinting the essential steric (structural) information onto the target protein: Lif structurally stabilizes an intermediate *Pa*LipA conformation, particularly a β-sheet in the region of residues 17-30, such that the opening of *Pa*LipA's lid domain is facilitated.

Acknowledgments

This study was supported by the Deutsche Forschungsgemeinschaft (DFG, German Research Foundation) through funding no. GO 1367/1-1 and INST 208/704-1 FUGG to HG and JA 448/8-1 to KEJ. Part of the work was funded by CRC 1208 (project A02 to FK and KEJ, and A03 to HG). HG is grateful for computational support and infrastructure provided by the "Zentrum für Informations- und Medientechnologie" (ZIM) at the Heinrich Heine University Düsseldorf and the computing time provided by the John von Neumann Institute for Computing (NIC) on the supercomputer JURECA at Jülich Supercomputing Centre (JSC) (user IDs: HKF7, HDD16; project IDs: 11237, 12732).

References

1. Nardini, M.; Lang, D. A.; Liebeton, K.; Jaeger, K.-E.; Dijkstra, B. W. J Biol Chem 2000.
2. Jaeger, K.-E.; Eggert, T. Curr Opin Biotechnol 2002, 13(4), 390-397.
3. Verger, R. Trends Biotechnol 1997, 15(1), 32-38.
4. Derewenda, Z. S. In Adv Protein Chem; Elsevier, 1994, p 1-52.
5. Jaeger, K.-E.; Reetz, M. T. Trends Biotechnol 1998, 16(9), 396-403.
6. Rosenau, F.; Jaeger, K.-E. Biochimie 2000, 82(11), 1023-1032.
7. Rosenau, F.; Tommassen, J.; Jaeger, K. E. ChemBioChem 2004, 5(2), 152-161.
8. Douzi, B.; Ball, G.; Cambillau, C.; Tegoni, M.; Voulhoux, R. J Biol Chem 2011, 286(47), 40792-40801.
9. El Khattabi, M.; Van Gelder, P.; Bitter, W.; Tommassen, J. J Biol Chem 2000, 275(35), 26885-26891.
10. Pauwels, K.; del Pino, M. M. S.; Feller, G.; Van Gelder, P. PLoS One 2012, 7(5), e36999.
11. Pauwels, K.; Van Molle, I.; Tommassen, J.; Van Gelder, P. Mol Microbiol 2007, 64(4), 917-922.
12. Sohl, J. L.; Jaswal, S. S.; Agard, D. A. Nature 1998, 395(6704), 817.
13. Pauwels, K.; Lustig, A.; Wyns, L.; Tommassen, J.; Savvides, S. N.; Van Gelder, P. Nat Struct Mol Biol 2006, 13(4), 374-375.
14. Noble, M.; Cleasby, A.; Johnson, L.; Egmond, M.; Frenken, L. FEBS Lett 1993, 331(1-2), 123-128.
15. Kelley, L. A.; Sternberg, M. J. E. Nature Protocols 2009, 4, 363.
16. Guex, N.; Peitsch, M. C. Electrophoresis 1997, 18(15), 2714-2723.
17. Mulnaes, D.; Gohlke, H. Journal of chemical theory and computation 2018, 14(11), 6117-6126.
18. Case, D.; Babin, V.; Berryman, J.; Betz, R.; Cai, Q.; Cerutti, D.; Darden, T.; Duke, R.; Gohlke, H.; Goetz, A. AMBER14 San Francisco: University of California 2014.
19. Maier, J. A.; Martinez, C.; Kasavajhala, K.; Wickstrom, L.; Hauser, K. E.; Simmerling, C. Journal of Chemical Theory and Computation 2015, 11(8), 3696-3713.
20. Ciglia, E.; Vergin, J.; Reimann, S.; Smits, S. H.; Schmitt, L.; Groth, G.; Gohlke, H. PLOS one 2014, 9(4), e96031.
21. Jorgensen, W. L.; Chandrasekhar, J.; Madura, J. D.; Impey, R. W.; Klein, M. L. J Chem Phys 1983, 79(2), 926-935.
22. Darden, T.; York, D.; Pedersen, L. J Chem Phys 1993, 98(12), 10089-10092.
23. Ryckaert, J. P.; Ciccotti, G.; Berendsen, H. J. C. J Comput Phys 1977, 23(3), 327-341.
24. Berendsen, H. J.; Postma, J. v.; van Gunsteren, W. F.; DiNola, A.; Haak, J. The Journal of chemical physics 1984, 81(8), 3684-3690.
25. Simmerling, C.; Strockbine, B.; Roitberg, A. E. J Am Chem Soc 2002, 124(38), 11258-11259.
26. Kumar, S.; Rosenberg, J. M.; Bouzida, D.; Swendsen, R. H.; Kollman, P. A. J Comput Chem 1992, 13(8), 1011-1021.
27. Roe, D. R.; Cheatham, T. E. Journal of Chemical Theory and Computation 2013, 9(7), 3084-3095.
28. Moradi, M.; Enkavi, G.; Tajkhorshid, E. Nature communications 2015, 6, 8393.
29. Pagani, G.; Gohlke, H. Scientific reports 2018, 8(1), 5733.
30. Chodera, J. D. Journal of chemical theory and computation 2016, 12(4), 1799-1805.
31. Welch, B. L. Biometrika 1947, 34(1/2), 28-35.
32. Fox, J.; Andersen, R. Department of Sociology, McMaster University 2005, 2-4.

33. Li, M. Z.; Elledge, S. J. In Gene synthesis; Springer, 2012, p 51-59.
34. Hausmann, S.; Wilhelm, S.; Jaeger, K. E.; Rosenau, F. FEMS Microbiol Lett 2008, 282(1), 65-72.
35. Jaeger, K.-E.; Kovacic, F. In Pseudomonas Methods and Protocols; Springer, 2014, p 111-134.
36. Pfleger, C.; Minges, A.; Boehm, M.; McClendon, C. L.; Torella, R.; Gohlke, H. Journal of Chemical Theory and Computation 2017, 13(12), 6343-6357.
37. Pfleger, C.; Rathi, P. C.; Klein, D. L.; Radestock, S.; Gohlke, H. Journal of Chemical Information and Modeling 2013, 53(4), 1007-1015.
38. Milić, D.; Dick, M.; Mulnaes, D.; Pfleger, C.; Kinnen, A.; Gohlke, H.; Groth, G. Scientific Reports 2018, 8(1), 3890.
39. Hermans, S. M.; Pfleger, C.; Nutschel, C.; Hanke, C. A.; Gohlke, H. Wiley Interdisciplinary Reviews: Computational Molecular Science 2017, 7(4), e1311.
40. Pfleger, C.; Gohlke, H. Structure 2013, 21(10), 1725-1734.
41. Pfleger, C.; Radestock, S.; Schmidt, E.; Gohlke, H. J Comput Chem 2013, 34(3), 220-233.
42. Mariani, V.; Biasini, M.; Barbato, A.; Schwede, T. Bioinformatics 2013, 29(21), 2722-2728.
43. Trodler, P.; Schmid, R. D.; Pleiss, J. BMC Struct Biol 2009, 9(1), 38.
44. Lee, H. S.; Oh, Y.; Kim, M.-J.; Im, W. The Journal of Physical Chemistry B 2018, 122(47), 10659-10668.
45. Joshi, D. C.; Lin, J. H. J Comput Chem 2019, 40(17), 1652-1663.
46. Lin, M. M.; Mohammed, O. F.; Jas, G. S.; Zewail, A. H. Proceedings of the National Academy of Sciences 2011, 108(40), 16622-16627.
47. De Sancho, D.; Best, R. B. J Am Chem Soc 2011, 133(17), 6809-6816.
48. El Khattabi, M.; Van Gelder, P.; Bitter, W.; Tommassen, J. J Mol Catal B: Enzym 2003, 22(5-6), 329-338.
49. Frenken, L.; Egmond, M. R.; Batenburg, A.; Bos, J. W.; Visser, C.; Verrips, C. T. Appl Environ Microbiol 1992, 58(12), 3787-3791.
50. Milic, D.; Dick, M.; Mulnaes, D.; Pfleger, C.; Kinnen, A.; Gohlke, H.; Groth, G. Sci Rep 2018, 8(1), 3890.
51. Rathi, P. C.; Fulton, A.; Jaeger, K.-E.; Gohlke, H. PLOS Comp Biol 2016, 12, e1004754.
52. Rathi, P. C.; Jaeger, K. E.; Gohlke, H. PLoS One 2015, 10(7), e0130289.
53. Gohlke, H.; Kiel, C.; Case, D. A. J Mol Biol 2003, 330, 891-913.
54. El Khattabi, M.; Ockhuijsen, C.; Bitter, W.; Jaeger, K.-E.; Tommassen, J. Molecular and General Genetics MGG 1999, 261(4-5), 770-776.
55. Cherukuvada, S. L.; Seshasayee, A. S. N.; Raghunathan, K.; Anishetty, S.; Pennathur, G. PLoS Comp Biol 2005, 1(3), e28.
56. Ferrario, V.; Ebert, C.; Knapic, L.; Fattor, D.; Basso, A.; Spizzo, P.; Gardossi, L. Adv Synth Catal 2011, 353(13), 2466-2480.
57. Johnson, Q. R.; Lindsay, R. J.; Nellas, R. B.; Shen, T. Proteins: Structure, Function, and Bioinformatics 2016, 84(6), 820-827.
58. Ciupka, D.; Gohlke, H. Scientific Reports 2017, 7(1), 8020.
59. Minges, A.; Ciupka, D.; Winkler, C.; Höppner, A.; Gohlke, H.; Groth, G. Scientific Reports 2017, 7, 45389.
60. Hutchinson, E. G.; Sessions, R. B.; Thornton, J. M.; Woolfson, D. N. Protein Sci 1998, 7(11), 2287-2300.
61. Merkel, J. S.; Sturtevant, J. M.; Regan, L. Structure 1999, 7(11), 1333-1343.

62. Wouters, M. A.; Curmi, P. M. G. Proteins: Structure, Function, and Bioinformatics 1995, 22(2), 119-131.
63. Bryan, P.; Wang, L.; Hoskins, J.; Ruvinov, S.; Strausberg, S.; Alexander, P.; Almog, O.; Gilliland, G.; Gallagher, T. Biochemistry 1995, 34(32), 10310-10318.
64. Jaswal, S. S.; Sohl, J. L.; Davis, J. H.; Agard, D. A. Nature 2002, 415(6869), 343.
65. Jaswal, S. S.; Truhlar, S. M.; Dill, K. A.; Agard, D. A. J Mol Biol 2005, 347(2), 355-366.
66. Jaeger, K.; Dijkstra, B.; Reetz, M. Annual Reviews in Microbiology 1999, 53(1), 315-351.